A Systematic Study of the Reactions of OH^- with Chlorinated Methanes. 1. Benchmark Studies of the Gas-Phase Reactions

Yurii A. Borisov

Nesmeynov Institute of Organo-Element Compounds, Russian Academy of Sciences, 117813 GSP-1, Vavilova Street 28, Moscow V-334, Russia

Edgar E. Arcia, Steven L. Mielke, Bruce C. Garrett,* and Thom H. Dunning, Jr.

Environmental Molecular Sciences Laboratory, Pacific Northwest National Laboratory, Richland, Washington 99352

Received: April 18, 2001; In Final Form: June 5, 2001

Ab initio electronic structure calculations and variational transition state theory are used to calculate reaction energetics and rate constants for the gas-phase reactions of OH^- with $CH_{(4-n)}Cl_n$ for $n = 1-4$. Two reaction pathways are considered, second-order (bimolecular) nucleophilic substitution (S_N2), and proton transfer. Benchmark electronic structure calculations using CCSD(T) and basis sets as large as aug-cc-pVQZ are performed to obtain highly accurate estimates of the enthalpies of reaction. These results are extrapolated to the complete basis set limit for comparison with experiment and to establish the level of theory needed to provide energies that are accurate to better than a few kJ/mol. Energies of critical geometries (reactant complexes, saddle points, and product complexes) are computed for all systems. For the S_N2 reaction, the potential energy and its first and second derivatives along minimum energy paths are computed and used directly in variational transition state theory (VTST) calculations of the rate constants. These calculations indicate that for $n = 1-3$ the region of the potential in the asymptotic reactant channel controls the reaction rate constants and that the loose-transition-state methods implemented in VARIFLEX provide the best estimates of the reaction rate constants. The reaction with $n = 4$ has a dynamical bottleneck that lies near the saddle point and is best treated using the VTST methods implemented in POLYRATE.

1. Introduction

Chlorinated hydrocarbons (CHCs) are one of the most common contaminants found at hazardous waste sites. Many of the chlorinated hydrocarbons are either known or suspected carcinogens and thus pose health risks to the public and/or site workers. Chlorinated hydrocarbons can undergo a variety of abiotic and biotic transformations.[1,2] Most abiotic processes such as hydrolysis and nucleophilic substitution are slow, but are still important on the time scale of the movement of CHCs in groundwater systems. As a result of the slowness of the reactions, few studies of the reactions of chlorinated hydrocarbons have been reported in the literature, and disagreement still exists about the mechanisms and rates of many of the key reactions. As an example, two estimates of the hydrolysis half-life of dichloromethane in water at 293 K differ by almost a factor of 500.[1]

Over the last several years, computational methods have advanced to the point that they are commonly used as a tool to predict rate constants for gas-phase reactions. However, the accurate prediction of rate constants for reactions in solution remains a challenge. Solvation can alter the reaction energetics, often dramatically, thereby changing the rate constants by orders of magnitude. In addition, solvent molecules can affect the dynamics of the reaction and alter the rate constants. Both the energetic and dynamic effects of the solvent can have contributions from long-range interactions from the bulk solvent as well as short-range interactions with solvent molecules near the reacting molecules.

Highly accurate ab initio electronic structure methods, which have been successful at predicting reaction energetics for gas-phase reactions, are too computationally demanding for modeling bulk phase systems. Although ab initio methods can be used to study short-range solvent interactions, approximate methods are required for estimating the effect of the long-range interactions on the reaction energetics. The approximate methods are physically well motivated, but the approximations have yet to be critically tested with benchmark calculations. A long-term goal of this research project is to use a systematic approach that builds up from first principle calculations to test these approximate methods.

The major objective of the research described here is to obtain accurate estimates of the lifetimes of CHCs in aqueous environments as determined by abiotic reactions and to identify any long-lived, potentially hazardous intermediates formed from the original CHCs. Estimating CHC lifetimes requires an understanding of the reaction mechanisms and knowledge of rate constants for all of the major reaction pathways. The systematic approach we propose begins with benchmark ab initio calculations on the gas-phase reactions. The focus of this work is on base-catalyzed hydrolysis reactions of chlorinated methane compounds, i.e., the reactions of OH^- with $CH_{(4-n)}Cl_n$ for $n = 1-4$. In the present paper we begin by providing benchmark calculations of the energetics of these reactions in the gas phase

* To whom correspondence should be addressed. Email: bruce.garrett@pnl.gov. Phone: (509) 376-1353. FAX: (509) 376-0420.

10.1021/jp011447c CCC: $20.00
Published on Web 07/18/2001

to understand the level of theory that is needed to accurately predict reaction energies and barrier heights. Future work will focus on the effects of solvation on the reaction energetics and rate constants.

We consider two pathways for the reaction of hydroxide ion with chlorinated methane compounds,

$$CH_{(4-n)}Cl_n + OH^- \rightarrow CH_{(4-n)}Cl_{(n-1)}OH + Cl^- \quad (R1)$$

$$CH_{(4-n)}Cl_n + OH^- \rightarrow CH_{(3-n)}Cl_n^- + H_2O \quad (R2)$$

Reaction R1 is a second-order (bimolecular) nucleophilic substitution (S_N2) reaction, and reaction R2 is a proton transfer (PT) reaction. A third reaction pathway, nucleophilic substitution to displace a hydride ion, has a reaction energy that is much higher than reactions R1 and R2 and is not considered here.

In addition to the environmental relevance of the aqueous-phase reactions of chlorinated methanes, reactions R1 and R2 in the gas phase are also of intrinsic interest. Gas-phase nucleophilic displacement reactions have received considerable attention for nearly 30 years,[3] and it has been observed that gas-phase S_N2 reactions can be as much as 20 orders of magnitude faster than those in aqueous solution.[4] The large effect of bulk solvation on reactions spurred interest in studies of the effect of small numbers of solvent molecules on the kinetics (i.e., the effect of microsolvation). Microsolvated versions of reaction R1 with $n = 1$ have been studied both experimentally[5−7] and theoretically.[8] The proton transfer reaction R2 is sufficiently endoergic in the gas phase that it has not been observed in thermal experiments. However, threshold energies have been measured for reaction R2 with $n = 1$ and for microsolvated versions of this reaction.[6,7] In the present work we compute rate constants for the gas-phase reactions for comparison to the experimental values of Staneke et al.[9]

The electronic aspects of S_N2 reactions in both gas and solution phases have been the subject of much research and a thorough overview has been given by Shaik et al.[10] Electronic structure calculations for the S_N2 gas-phase $OH^- + CH_3Cl$ reaction have been previously reported,[8,11] and more recently the reaction energies for chlorinated methanes with aqueous monovalent anions have been reported.[12] In the present work, we extend these previous calculations in several ways. First, the level of theory used in the present calculations to study reaction complexes and saddle points, as well as overall reaction energies, is higher than was possible 10 years ago. Second, we study the effects of chlorination on the energetics of reaction complexes, saddle points, and overall reaction. Third, we study the competition between the S_N2 and proton-transfer reactions. Although the PT reaction is uphill in energy by about 30 kJ/mol for CH_3Cl, it is downhill in energy by about 60 and 135 kJ/mol for CH_2Cl_2 and $CHCl_3$, respectively. In addition, the reaction of OH^- with chloroform is believed to proceed by the PT reaction.[9] Fourth, we present the S_N2 rate constants for reactions of OH^- with CH_3Cl and CCl_4, and total rate constants (summed over S_N2 and PT channels) for reactions of OH^- with CH_2Cl_2 and $CHCl_3$ and compare them with experimental results.[9]

2. Theoretical Methods

2.1. Electronic Structure Theory. The ab initio electronic structure calculations reported here used Møller−Plesset perturbation theory[13] through second order (MP2), third order (MP3), and fourth order (MP4), coupled cluster theory[14] with single and double excitations (CCSD) and with perturbative treatment of triple excitations [CCSD(T)], and the augmented correlation consistent polarized valence basis sets[15] for double-, triple-, and quadruple-ζ levels (i.e., aug-cc-pVDZ, aug-cc-pVTZ, and aug-cc-pVQZ). All critical geometries for reactions R1 and R2 were optimized at the MP2/aug-cc-pVDZ level. Single-point MP2, MP3, MP4, CCSD, and CCSD(T) calculations with the correlation consistent basis sets through quadruple-ζ level were then carried out to test the convergence of the computed energies with respect to the level of basis set and recovery of correlation energy.

Energies at the complete basis set (CBS) limit are approximated by extrapolation of total energies using the functional form[16]

$$E_x^Y = E_\infty^Y + A^Y e^{-(x-1)} + B^Y e^{-(x-1)^2} \quad (1)$$

where $x = 2, 3, 4$ for the double-, triple-, and quadruple-ζ basis sets and Y is the MP2, MP3, MP4, CCSD, or CCSD(T) method. Equation 1 represents a set of three linear equations for the three parameters (E_∞^Y, A^Y, and B^Y) and can be trivially solved to give expressions for these three parameters in terms of the three values of the energy E_x^Y for $x = 2$, 3, and 4. The extrapolated value of the energy can then be expressed as

$$E_\infty^Y = \sum_{x=2}^{4} C_x E_x^Y \quad (2)$$

where C_x are constants that do not depend on the level of theory Y and only depend on the functional form used in the extrapolation. For the functional form used in eq 1, the parameters C_2, C_3, and C_4 have the values 0.03486711, −0.71162243, and 1.67675533, respectively. CCSD(T)/aug-cc-pVQZ calculations, particularly for systems with multiple chlorine atoms, are expensive to perform routinely, so we explore methods to approximate the CBS limit for CCSD(T) using lower level calculations. One approach is to write the CCSD(T) CBS limit in terms of the CBS limit for a lower level of theory, Y, and the difference between the CBS limits of CCSD(T) and theory Y

$$E_\infty^{CCSD(T)} = E_\infty^Y + (E_\infty^{CCSD(T)} - E_\infty^Y) \quad (3)$$

The difference is then approximated based upon convergence of a lower level of theory. To do this we rewrite the CBS limit for level Y as

$$E_\infty^Y = E_3^Y + \gamma^Y(E_3^Y - E_2^Y) \quad (4)$$

where by definition

$$\gamma^Y = (E_\infty^Y - E_3^Y)/(E_3^Y - E_2^Y) \quad (5)$$

Assuming the difference between CCSD(T) and theory Y converges at the same rate (with respect to basis set) as theory Y, we can approximate eq 3 by

$$E_\infty^{CCSD(T)} \approx E_\infty^Y + E_3^{CCSD(T)} - E_3^Y + \gamma^Y(E_3^{CCSD(T)} - E_3^Y - E_2^{CCSD(T)} + E_2^Y) \quad (6)$$

Using eq 4, this expression can be rewritten as

$$E_\infty^{CCSD(T)} \approx E_\infty^{CCSD(T)||Y} = E_3^{CCSD(T)} + \gamma^Y(E_3^{CCSD(T)} - E_2^{CCSD(T)}) \quad (7)$$

where we introduce the notation CCSD(T)||*Y* to denote that the CBS extrapolation of CCSD(T) is assumed to converge at the same rate as theory *Y* and can be approximated by the simple two-point extrapolation formula given in eq 7. The extrapolation approximation of eq 7 is similar in spirit to an additivity approximation recently studied by Dunning and Peterson,[17] in which the CCSD(T) energy obtained with a higher basis set (e.g., augmented quintuple-ζ quality) is approximated from CCSD(T) with a smaller basis (e.g., augmented triple-ζ quality) and the difference between MPn calculations with the quintuple-ζ and triple-ζ basis sets. They found that using MP3 in this approximation gave a good compromise of accuracy and computational effort. The approximation in eq 7 will be tested for stationary points on the potential energy surfaces for these reactions in a later section.

The electronic structure calculations were carried out using the GAUSSIAN98,[18] MOLPRO,[19] and NWCHEM[20] program packages. The larger calculations (e.g., CCSD(T)/aug-cc-pVQZ) were performed using NWCHEM on multiple processors (typically 128) of the IBM SP in the Molecular Science Computing Facility. The largest calculations involved 542 basis functions.

2.2. Variational Transition State Theory. Reaction rate constants are calculated using variational transition state theory (VTST)[21,22] as implemented in POLYRATE[23] and using phase-space-integral-based VTST (PSI−VTST)[24] as implemented in VARIFLEX,[25] which is appropriate for treating loose transition states found in barrierless association reactions and unimolecular reactions. Details for such calculations are presented in the references cited above, so we only provide a brief summary and focus on the information about the potential energy surface that is needed to compute the rate constants. The VTST expression for the rate constant takes the form

$$k^{GT}(T,\boldsymbol{\sigma}) = \frac{k_B T}{h} K^0 \exp[-\Delta G^{GT}(T,\boldsymbol{\sigma})/k_B T] \qquad (8)$$

where T is the temperature, $\boldsymbol{\sigma}$ is a collection of parameters defining the transition-state dividing surface, k_B is Boltzmann's constant, h is Planck's constant, K^0 defines the standard state, which we choose as 1 cm^3 molecule^{-1}, and $\Delta G^{GT}(T,\boldsymbol{\sigma})$ is the generalized transition-state free energy of activation. In POLYRATE the dividing surfaces are chosen to be planes perpendicular to the reaction coordinate and $\boldsymbol{\sigma}$ represents the single parameter s, which is the distance along the minimum energy path (MEP). The reaction coordinate is taken to be the MEP, or path of steepest descent in mass-weighted coordinates from the saddle point. In the PSI−VTST calculations using VARIFLEX, the dividing surface is defined in terms of the distance between pivot points on each reactant species (e.g., $CH_{(4-n)}Cl_n$ and OH^-) and the geometries of the molecules at those pivot points. In our calculations the pivot points are taken as the centers of mass of the two species, and $\boldsymbol{\sigma}$ represents the single parameter, the center of mass separation R. For fixed values of the molecular geometries, the distance between the pivot points is the reaction coordinate in these calculations. The generalized transition-state free energy of activation is given by

$$\Delta G^{GT}(T,\boldsymbol{\sigma}) = V_{MEP}(\boldsymbol{\sigma}) - k_B T \ln[Q^{GT}(T,\boldsymbol{\sigma})/K^0 \Phi^R(T)] \quad (9)$$

where $V_{MEP}(\boldsymbol{\sigma})$ is the potential along the reaction coordinate, $Q^{GT}(T,\boldsymbol{\sigma})$ is the generalized transition-state partition function, and $\Phi^R(T)$ is the reactant partition function per unit volume. In canonical variational transition state theory (CVT) the transition-state dividing surface is optimized to find the dynamical bottleneck where the thermal rate constant is a minimum. This is equivalent to maximizing the activation free energy with respect to the parameters $\boldsymbol{\sigma}$ that define the dividing surface. For the CVT calculation the location of the reaction coordinate at the variational dividing surface is defined as s^*_{CVT}. For the PSI−VTST calculations, the location of the reaction coordinate at the variational dividing surface is defined as R^*_{PSI}.

The reactant partition function is treated as a product of rotational, vibrational, and translational partition functions. The rotational and translational partition functions are treated classically, and the vibrational partition functions are approximated by the product of quantum mechanical harmonic oscillator partition functions for independent normal modes. For the case studied here there is one vibrational mode for OH^- and nine vibrational modes for $CH_{(4-n)}Cl_n$. The transition-state partition functions are treated as a product of rotational and vibrational partition functions, where the rotational partition functions are treated classically.

In the generalized transition state complex there are 14 vibrational modes, 10 that correlate with the bound vibrations in reactants and four transitional modes that evolve from free rotations in reactants to hindered rotors along the reactant entrance channel and finally become bend vibrations in the reactant complex. The vibrational partition functions are approximated by the product of the partition function for the 4 transitional modes with the partition function for the 10 vibrational normal modes that correlate with the bound vibrations in reactants. The partition functions for the 10 vibrations are treated in the same manner as in reactants, e.g., quantum mechanically, as independent harmonic normal modes. For generalized transition states with sufficiently small CO separation, the vibrational frequencies of the four transitional modes are high enough that a quantum mechanical treatment is appropriate. In this case we calculate the partition functions quantum mechanically using the independent normal mode harmonic oscillator approximation. For reactions in which the dynamical bottleneck is in the asymptotic reactant region and the transitional modes are hindered or nearly free rotational motion, a more accurate approach is to approximate the partition function classically for the transitional modes. This is the approach used in the phase-space-integral-based formulation of VTST,[24] in which the multidimensional phase-space averages are computed analytically for the momentum integrals and numerically for the configurational integrals.

The VTST calculations using POLYRATE require calculation of the minimum energy pathway and values of the potential energy and its first and second derivatives along the MEP. These calculations employed direct dynamics techniques[26] in which the energies, gradients, and Hessians from electronic structure calculations are used directly in the rate constant calculation without fitting them first to an analytical functional form. For most of the reactions, the potential along the MEP displays a double well, with the intermediate barrier below the reactant asymptote. The MEP near the saddle point is found by following the path of steepest descent from the saddle point on both the reactant and product sides. The MEP in the asymptotic reactant region is found by starting at a geometry in the reactant valley in which the distance between the centers of mass of OH^- and $CH_{(4-n)}Cl_n$ is constrained and all other coordinates are optimized. The path of steepest descent is followed from this point into the well. Different starting points in the asymptotic valleys (progressively further out) were used to test the convergence of the MEP in the asymptotic regions.

Another useful quantity used in the VTST calculations as implemented in POLYRATE is the ground-state adiabatic potential curve, which for the reactions studied here is defined by

$$V_a^G(T,s) = V_{MEP}(s) + \sum_{m=1}^{14} \epsilon_{m,0}^{GT}(s) \qquad (10)$$

where $\epsilon_{m,0}^{GT}(s)$ is the ground-state generalized transition-state vibrational energy for mode m, and we have indicated that the sum is over the 14 vibrational modes in the generalized transition state complex. The ground-state adiabatic potential curve is the zero-temperature limit of the generalized transition-state free energy of activation curve (to within an additive constant), and it can help identify the location of the dynamical bottleneck for a reaction. In addition, the ground-state adiabatic potential curve is the appropriate potential for calculating tunneling corrections in VTST.[22] If the adiabatic potential along the reaction path is equal to or below the maximum of its values in the asymptotic reactant and product channels, then there is no intrinsic barrier to reaction and tunneling is not important. At reactants, $V_{MEP}(s)$ goes to zero (by definition) and the adiabatic potential goes to the reactant zero-point energy. The relative ground-state adiabatic potential is defined by

$$\Delta V_a^G(T,s) = V_{MEP}(s) + \sum_{m=1}^{14} \epsilon_{m,0}^{GT}(s) - \sum_{m=1}^{10} \epsilon_{m,0}^{R} \qquad (11)$$

where $\epsilon_{m,0}^{R}$ is the reactant ground-state vibrational energy for mode m, and we have indicated that the sum is over the 10 vibrational modes in reactants (the four transitional modes become free rotations in the asymptotic reactant region and their ground-state energy levels go to zero). In section 3.4 we present the $\Delta V_a^G(T,s)$ curves and show that they do not exhibit any intrinsic barriers; therefore, tunneling is not important for the reactions studied here and we do not include corrections for quantum mechanical motion along the reaction coordinate in the calculated rate constants reported in this paper. Note however that quantum mechanical effects are included for bound vibrational motion when appropriate.

Energy profiles along the MEP can also be used in calculations of rate constants for barrierless ion−molecule association reactions as implemented in VARIFLEX. Alternatively, V_{MEP} in the asymptotic region can be approximated using an electrostatic model based upon a multipole expansion. The electrostatic model also provides an analytical expression for the potential in the calculation of the partition functions for the transitional modes. More details of the fits to the electrostatic potential and subsequent rate constant calculations are presented below. We note that the use of a simple electrostatic potential in rate-constant calculations for ion−molecule reactions is well documented in the literature.[27,28] For ion−dipole interactions, the Langevin model[27] places transition states at centrifugal barriers for spherically symmetric approximations to the ion−dipole potential. This simple approach can break down from asymmetries in the long-range potential and has been extended using variational transition state theory by Bowers, Chesnavich, and Su.[28] The phase-space-integral based VTST approach employed here is a significant improvement over these previous approaches by including a more accurate treatment of the potential and by accurate calculation of partition functions for the transitional modes.

3. Results and Discussion

Total energies for reactants, products, complexes, and saddle points are provided in Tables S1−S7 of the Supporting Information. Summaries of the relative energies are provided in the following two sections.

TABLE 1: Experimental Heats of Formation and Approximate Zero-Point Energies for Reactants and Products of Reactions R1 and R2

molecule	$\Delta_f H°$ (kJ/mol) (0 K)	$\Delta_f H°$ (kJ/mol) (298 K)	zero-point energy[a] (kJ/mol)
OH^-	-137.4 ± 3.8[b]	-143.6 ± 3.8[b]	22.5
Cl^-	-229.4 ± 0.4[b]	-234.0[b]	
H_2O	-238.92 ± 0.04[b]	-241.83 ± 0.04[b]	56.0
CH_3Cl	-74.0 ± 0.6[c]	-81.9 ± 0.5[d]	99.8
CH_2Cl_2	-88.5 ± 1.1[c]	-95.4 ± 1.1[d]	77.8
$CHCl_3$	-98.0 ± 1.4[c]	-102.7 ± 1.2[d]	52.8
CCl_4	-93.7 ± 1.1[c]	-95.7 ± 1.0[d]	25.6
CH_3OH	-190.1 ± 1.2[c]	-200.9 ± 0.2[d]	135.4
CH_2ClOH	-239 ± 8[e]	-250 ± 7[f]	114.4
$CHCl_2OH$	-259 ± 7[e]	-268 ± 6[f]	89.5
CCl_3OH	-280 ± 7[e]	-286 ± 6[f]	61.8
CH_2Cl^-	55 ± 16[e]	45 ± 16[g]	58.9
$CHCl_2^-$	-51 ± 17[e]	-59 ± 17[g]	38.8
CCl_3^-	-135 ± 28[e]	-141 ± 28[g]	14.3

[a] Vibrational zero-point energy estimated using harmonic frequencies from MP2/aug-cc-pVDZ calculations. [b] Experimental value from JANAF Thermochemical Tables.[29] [c] Experimental value from "Thermodynamics of Organic Compounds in the Gas State".[31] Note that error bars are not reported in this reference. See text for discussion of error bars for these values. [d] Experimental value from "Thermochemical Data and Structures of Organic Compounds".[30] [e] Obtained from $\Delta_f H°$ (298 K) and an estimate of $\Delta_f H°$(298 K) − $\Delta_f H°$(0 K). (See text). [f] Values obtained from calculations of heats of reaction for isodesmic reactions.[12] [g] Experimental value from "Gas-Phase Ion and Neutral Thermochemistry".[32]

3.1. Benchmark ab Initio Electronic Structure Calculations for Reaction Energies. One calibration of the electronic structure methods is provided by comparing the computed reaction energies for reactions R1 and R2 with experimental values. The calculated reaction energies ΔE_{rxn} are the difference in classical energies (without zero-point energy contributions) between the products and reactants. For comparison with experiment, we obtain computed heats of reactions at 0 K, ΔH_{rxn}(0 K), by adding zero-point energy differences to the computed reaction energies. The zero-point energies are approximated using harmonic frequencies obtained from MP2/aug-cc-pVDZ calculations.

The experimental values for ΔH_{rxn}(0 K) are computed using experimental heats of formation, $\Delta_f H°$(0 K), for the reactant and product species. The experimental heats of formation and computed zero-point energies, which we use to approximate the computed heats of reaction, are summarized in Table 1. The heats of formation for OH^- and Cl^- are taken from the JANAF Thermochemical Tables.[29] The heats of formation at 298 K for CH_3Cl, CH_2Cl_2, $CHCl_3$, CCl_4, and CH_3OH are obtained from Pedley.[30] Values for these five molecules are also reported by Frenkel et al.[31] for 0 and 298 K, but without error bars. At 298 K the values of Frenkel et al. (−82.0, −95.4, −102.9, −95.8, and −200.9 kJ/mol respectively for the five molecules listed above) are within 0.2 kJ/mol of those of Pedley in all cases. For the chlorinated methane molecules, values are also reported in the JANAF Tables for both 0 and 298 K. The JANAF values at 298 K (-83.7 ± 2.1, -95.5 ± 1.3, -103.2 ± 1.3, -95.8 ± 2.1 kJ/mol for CH_3Cl, CH_2Cl_2, $CHCl_3$, and CCl_4, respectively) have larger deviations from the Pedley values, but the latter are seen to be within the larger error bars of the JANAF values. Since the values of Frenkel et al. agree well with Pedley at 298 K, we use the values of Frenkel et al. at 0 K and assign errors bars equal to the Pedley error bar at 298 K.

TABLE 2: Reaction Enthalpies, ΔH_{rxn}(0 K), for the S_N2 Reactions R1 of $OH^- + CH_{(4-n)}Cl_n$ for $n = 1-4$

		ΔH_{rxn}(0 K) (kJ/mol)			
n	method	aug-cc-pVDZ	aug-cc-pVTZ	aug-cc-pVQZ	CBS[a]
1	MP2	−203.1	−192.5	−193.1	−193.9
	MP3	−230.3	−223.6	−226.5	−228.7
	CCSD	−218.9	−212.4	−215.5	−217.9
	CCSD(T)	−211.3	−203.6	−206.4	−208.6
	exptl[b]				−208 ± 8
2	MP2	−233.6	−222.7	−223.2	−223.9
	MP3	−263.2	−256.8	−259.9	−262.1
	CCSD	−250.4	−244.1	−247.4	−249.8
	CCSD(T)	−242.6	−235.2	−238.1	−240.3
	exptl[b]				−246 ± 13
3	MP2	−255.7	−244.1	−244.6	−245.3
	MP3	−288.9	−282.3	−285.4	−287.7
	CCSD	−273.8	−267.3	−270.8	−273.3
	CCSD(T)	−265.8	−258.0	−261.0	−263.3
	exptl[b]				−255 ± 12
4	MP2	−260.3	−249.8	−249.8	−250.2
	MP3	−297.7	−292.7	−295.4	−297.3
	CCSD	−280.5	−275.6	−278.7	−280.9
	CCSD(T)	−271.7	−265.5	−268.0	−269.9
	exptl[b]				−279 ± 12

[a] Complete basis set limit for the reaction enthalpy is obtained by using eq 1 and adding zero-point contributions from harmonic frequencies at the MP2/aug-cc-pVDZ level. [b] Experimental reaction enthalpy obtained from $\Delta_f H°$(0 K) values in Table 1.

Experimental values of $\Delta_f H°(T)$ for the chlorinated methanol molecules are not available. The values listed in Table 1 at 298 K are obtained from electronic structure calculations of heats of reaction for isodesmic reactions.[12] Error bars include experimental uncertainties of the compounds used in the isodesmic reactions and assume ±4 kJ/mol error in the calculated heat of reaction. We approximate $\Delta_f H°$(0 K) for these molecules using these values at 298 K and $\Delta_f H°$(298 K) − $\Delta_f H°$(0 K) estimated by using calculational methods from the JANAF tables and harmonic vibrational frequencies from MP2/aug-cc-pVDZ calculations.

The values of $\Delta_f H°$(298 K) for the chlorinated methyl anions are available from Lias et al.[32] We approximate $\Delta_f H°$(0 K) for these molecules by the same method used for the chlorinated methanol molecules.

To obtain the error bars for $\Delta_f H°$(0 K), we added an estimate of the uncertainty in the vibrational contribution to $\Delta_f H°$(298 K) − $\Delta_f H°$(0 K). The computed zero-point energies listed in Table 1 can also be compared with approximate experimental ones for some of the molecules. For OH^-, the zero-point energy can be approximated from spectroscopic constants, and for H_2O and the chlorinated methane compounds, it can be approximated harmonically from fundamental frequencies taken from the JANAF Tables.[29] In these cases the zero-point energies computed from the MP2/aug-cc-pVDZ calculations agree with those obtained from experimental considerations to better than 4 kJ/mol. Since the vibrational contribution to $\Delta_f H°$(298 K) − $\Delta_f H°$(0 K) is typically less than one-fourth of the total, we use a value of ±1 kJ/mol for the vibrational contribution to the error bar.

The computed and experimental reaction enthalpies are compared in Table 2 for reaction R1 and Table 3 for reaction R2. Error bars on the experimental values reflect uncertainties in the values for $\Delta_f H°$(0 K) for both reactants and products. The data are also shown in Figures 1 and 2, where the convergence to the complete basis set limit is depicted. Values of the extrapolations to the complete basis set (CBS) limit are obtained as follows. The total energies were summed over all reactant (e.g., OH^-, CH_3Cl, etc.) or product (e.g., Cl^-, CH_3OH, etc.) fragments, and then extrapolated using the functional form given in eq 1.

TABLE 3: Reaction Enthalpies, ΔH_{rxn}(0 K), for the Proton Transfer Reactions R2 of $OH^- + CH_{(4-n)}Cl_n$ for $n = 1-3$

		ΔH_{rxn}(0 K) (kJ/mol)			
n	method	aug-cc-pVDZ	aug-cc-pVTZ	aug-cc-pVQZ	CBS[a]
1	MP2	38.7	40.9	40.1	39.5
	MP3	13.5	14.3	12.8	11.8
	CCSD	22.1	24.4	23.2	22.2
	CCSD(T)	23.4	26.3	25.1	24.3
	exptl[b]				27 ± 21
2	MP2	−44.9	−38.8	−40.1	−41.1
	MP3	−72.0	−67.4	−69.9	−71.7
	CCSD	−63.3	−56.9	−59.0	−60.6
	CCSD(T)	−62.9	−56.7	−58.8	−60.5
	exptl[b]				−64 ± 23
3	MP2	−121.2	−111.7	−113.0	−114.3
	MP3	−146.4	−137.5	−140.4	−142.7
	CCSD	−136.9	−126.5	−129.0	−131.0
	CCSD(T)	−139.8	−130.3	−133.1	−135.4
	exptl[b]				−139 ± 34

[a] Complete basis set limit for the reaction enthalpy is obtained by using eq 1 and adding zero-point contributions from harmonic frequencies at the MP2/aug-cc-pVDZ level. [b] Experimental reaction enthalpy obtained from $\Delta_f H°$(0 K) values in Table 1.

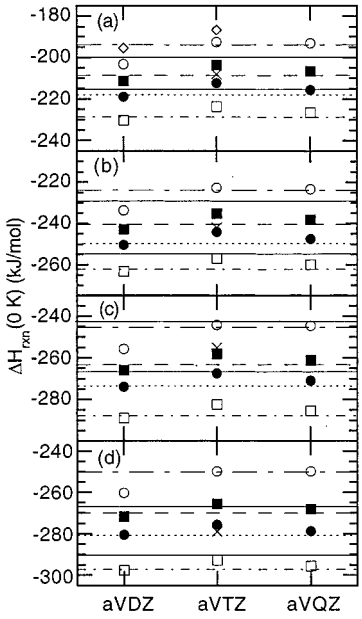

Figure 1. Convergence with respect to basis set of the reaction enthalpy for the S_N2 reaction $CH_{(4-n)}Cl_n + OH^- \rightarrow CH_{(4-n)}Cl_{(n-1)}OH + Cl^-$. Parts a−d are for $n = 1-4$, respectively. Open circles, squares, and diamonds denote the results of MP2, MP3, and MP4 calculations, respectively. Filled circles and squares denote the results of CCSD and CCSD(T) calculations, respectively. The long dash-short dash lines and medium dash-short dash lines are the CBS extrapolations for MP2 and MP3, respectively. The dotted lines and long dash lines are the CBS extrapolations for CCSD and CCSD(T), respectively. The crosses are the best experimental estimates and the two thin horizontal solid lines in each part denote the error bars on the experimental value.

For the S_N2 reaction with CH_3Cl, CH_2Cl_2, and $CHCl_3$, CCSD(T) is the only method that gives a CBS extrapolation of the reaction enthalpy lying within the experimental uncertainty for all the reactions. Compared to the best experimental estimate for these three reactions, the CCSD(T) CBS results range from 4 kJ/mol higher to 13 kJ/mol lower. The MP2 extrapolations

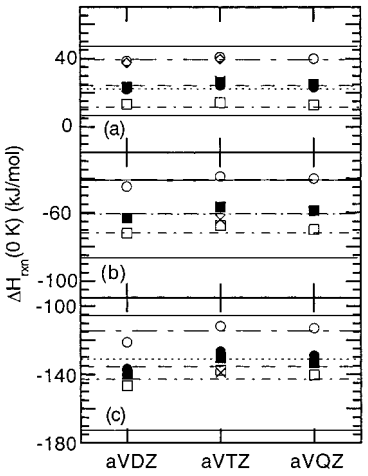

Figure 2. Same as Figure 1, except for the proton-transfer reaction $CH_{(4-n)}Cl_n + OH^- \rightarrow CH_{(3-n)}Cl_n^- + H_2O$. Parts a−c are for $n = 1-3$, respectively.

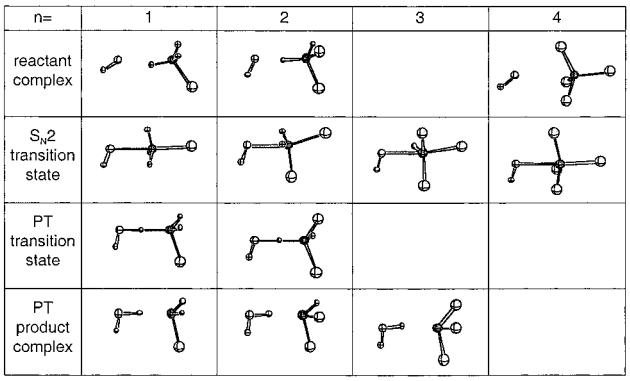

Figure 3. Geometries of reactant complex, S_N2 saddle point, proton-transfer saddle point, and proton-transfer product complex for the $OH^- + CH_{(4-n)}Cl_n$ reactions for $n = 1-4$. Blank entries indicate that critical geometries were not located in these cases. Small white, small gray, black, and large gray spheres are H, O, C, and Cl atoms, respectively.

are consistently too high and are outside the experimental error bars for three of the four S_N2 reactions, while the MP3 extrapolations are consistently too low and are outside the experimental range in all cases. Compared to the best experimental estimates, the MP3 values are 22 to 37 kJ/mol lower.

The experimental error bars on the reaction enthalpies for the proton-transfer reactions are much larger because of the large uncertainties in the heats of formation of the $CH_{(3-n)}Cl_n^-$ species. The MP3, CCSD, and CCSD(T) methods give extrapolated CBS values that are within the experimental range for all three PT reactions, and MP2 gives CBS values that are within the experimental range in all cases except the reaction with CH_2Cl_2. The CCSD and CCSD(T) methods give surprisingly similar reaction enthalpy estimates; thus, the effects of the *connected* triple excitations in reactants and products must nearly cancel. As for the S_N2 reactions, the CCSD(T) CBS extrapolation gives the best agreement with the experimental estimates, giving values that are within 3.4 kJ/mol for all three proton-transfer reactions. The MP3 CBS extrapolations are 6 to 16 kJ/mol lower than the best experimental estimates.

Hierl et al.[6] have reported a threshold energy of 0.36 eV or 35 kJ/mol for the proton-transfer reaction in $OH^- + CH_3Cl$. If there is no free-energy barrier along the reaction coordinate in the exit channel for this reaction, then the threshold energy should be the same as $\Delta H_{rxn}(0\ K)$. The threshold energy is within the experimental error bars for $\Delta H_{rxn}(0\ K)$, but it is 8 kJ/mol higher than the best experimental estimate and 11 kJ/mol higher than the best theoretical estimate. It would be interesting to characterize the exit channel more accurately for this reaction to get a better theoretical estimate of the threshold energy and to see if it differs appreciably from the reaction enthalpy.

3.2. Reaction Complexes and Saddle Points. Figure 3 presents the structures of the bound complexes and saddle points for reactions R1 and R2 computed at the MP2/aug-cc-pVDZ level of theory. For the reactions of CH_3Cl and CH_2Cl_2 ($n = 1-2$), we located the reactant complexes (with the OH^- hydrogen bonded to one of the protons on the chlorinated methane), the saddle points for the S_N2 reactions, the saddle points for the PT reactions, and the product complexes for the PT reactions (with H_2O hydrogen bonded to the chlorinated methyl anion). For the reaction with chloroform ($n = 3$) we could not locate a reactant complex or a PT saddle point at the MP2/aug-cc-pVDZ level of theory; only the S_N2 saddle point and PT product complex were located. The absence of the reactant complex and PT saddle point are discussed in more detail below. For carbon tetrachloride ($n = 4$) the proton transfer channel is not available and only the reactant complex and S_N2 saddle point were located.

In going from $n = 1$ to 2 for the $OH^-\cdots CH_{(4-n)}Cl_n$ reactant complex, the distance between the O atom and the donor H atom on the methane molecule decreases from 1.77 to 1.51 Å, and the CH bond for the donor proton lengthens from 1.12 to 1.19 Å. This change in bond length is consistent with the protons on $CH_{(4-n)}Cl_n$ becoming more acidic with increasing numbers of chlorine atoms. The CCl bond lengths of 1.83 and 1.82 Å are nearly the same for $n = 1$ and 2, respectively.

For $n = 4$, the lack of protons on the carbon tetrachloride molecule leads to a different orientation of OH^- with the O atom making a nearly symmetric approach to a triangular face of three of the Cl atoms in CCl_4. The CO distance is 3.1 Å, and the CCl distance is 1.83 Å for the Cl atom furthest from the O atom. This orientation is more similar to the S_N2 saddle points. In the S_N2 saddle points, the CO distances are shorter—2.24, 2.18, 2.18, and 2.29 Å for $n = 1-4$, respectively; the CCl distances are longer: 2.06, 2.09, 2.14, and 2.06 Å, respectively. Notice that in going from $n = 1$ to 3, the CO distance decreases while the CCl distance increases. For the reaction with CH_3Cl, the OH^- species is oriented so that the H on the OH^- is gauche with respect to the methyl group. In the reactions with CH_2Cl_2 and $CHCl_3$, the H on the OH^- is cis to the Cl atom that is not displaced. For $n = 4$ the saddle point geometry is more similar to that for $n = 1$.

For the PT saddle points, the O, H, and C atoms (where *H* is the proton being transferred from C to O) are nearly collinear. For $n = 1$ and 2, the OH bond distances are 1.15 and 1.31 Å, respectively, and the HC bond distances are 1.51 and 1.31 Å, respectively. In both cases, the H on the OH^- is cis to one of the Cl atoms on the methane molecule. In the PT product complexes with $n = 1-3$, the OH distances for the proton donor in water are 1.06, 1.03, and 1.01 Å, respectively, and the HC distances for the donor H atom from water are 1.69, 1.79, and 1.86 Å, respectively. Thus, the OH distance decreases and the HC distances increase as Cl atoms are added and stabilize the methyl anion.

Note that for $n = 1$ and 2, the orientations in the reactant complex and PT saddle point are nearly the same. For the reactant complex, the OH distance in the hydrogen bond decreases by 0.26 Å in going from $n = 1$ to 2. Another 0.2 Å decrease in going from $n = 2$ to 3 yields an OH bond length of

TABLE 4: Energies of Bound Complexes $OH^-\cdots CH_{(4-n)}Cl_n$ Relative to Energies of Reactants $OH^- + CH_{(4-n)}Cl_n$ for $n = 1$, 2, and 4

		ΔE (kJ/mol)			
n	method	aug-cc-pVDZ	aug-cc-pVTZ	aug-cc-pVQZ	CBS[a]
1	MP2	−68.6	−66.4	−66.0	−65.8
	MP3	−70.7	−69.4	−69.4	−69.5
	CCSD	−68.2	−66.2	−65.9	−65.8
	CCSD(T)	−70.7	−68.6	−68.1	−67.9
2	MP2	−105.5	−100.8	−100.5	−100.4
	MP3	−108.2	−104.5	−104.7	−105.0
	CCSD	−103.6	−98.9	−98.7	−98.7
	CCSD(T)	−108.3	−103.5	−103.3	−103.2
4	MP2	−34.2	−36.7	−36.8	−36.8
	MP3	−32.5	−35.0	−35.3	−35.4
	CCSD	−32.3	−34.2	−34.2	−34.1
	CCSD(T)	−35.8	−38.3	−38.5	−38.5

[a] Complete basis set limit for the relative energy is obtained by using eq 1.

TABLE 5: Energies of Bound Complexes $CH_{(3-n)}Cl_n^-(H_2O)$ Relative to Energies of Reactants $OH^- + CH_{(4-n)}Cl_n$ for $n = 1-3$

		ΔE (kJ/mol)			
n	method	aug-cc-pVDZ	aug-cc-pVTZ	aug-cc-pVQZ	CBS[a]
1	MP2	−45.8	−43.8	−43.6	−43.5
	MP3	−61.7	−61.4	−61.7	−61.8
	CCSD	−52.7	−50.7	−50.5	−50.5
	CCSD(T)	−55.8	−53.8	−53.5	−53.3
2	MP2	−116.5	−111.4	−111.5	−111.8
	MP3	−135.7	−132.1	−133.1	−133.9
	CCSD	−126.3	−120.8	−121.3	−121.8
	CCSD(T)	−129.5	−124.2	−124.6	−125.1
3	MP2	−179.9	−171.6	−171.9	−172.3
	MP3	−198.4	−190.9	−192.2	−193.4
	CCSD	−188.6	−179.3	−180.1	−180.9
	CCSD(T)	−193.8	−185.1	−186.0	−186.9

[a] Complete basis set limit for the relative energy is obtained by using eq 1.

1.31 Å. However, this is the same distance as seen in the PT saddle point for $n = 2$, indicating that the geometry for the reactant complex may be near the saddle point for the PT reaction (if it exists) for $n = 3$. Also, the location of the transferring proton in the PT saddle point becomes earlier (closer to the reactant complex) in going from $n = 1$ to 2, with a decrease in HC bond length of 0.2 Å. If another 0.2 Å increase occurs with addition of another Cl atom, the HC distance would be nearly the equilibrium CH bond length in chloroform. The progressions of the bond lengths in the reactant complexes and in the PT saddle points in the $OH^- + CH_3Cl$ and CH_2Cl_2 reactions suggest that the $OH^- + CHCl_3$ reaction may proceed monotonically downhill in energy from reactants to the PT product complex. It is interesting that the S_N2 saddle point for the $n = 3$ reaction is still observed even though the reactant complex is not. The minimum energy path was followed from this saddle point in the reactant direction and it was found to go to the proton-transfer complex.

The energies of the bound complexes and saddle points, relative to the reactant minimum energies, are presented in Tables 4−7 for several levels of theory. For the reactant complexes, the convergence to the complete basis set limit is excellent for the MP2 and MP3 methods; the CBS values are within 0.3 kJ/mol of the aug-cc-pVQZ results in all cases. In addition, the agreement between the MP2, MP3, CCSD, and CCSD(T) methods is quite good; the MP3 and CCSD(T) results

TABLE 6: Barrier Heights for the S_N2 Reactions R1 of $OH^- + CH_{(4-n)}Cl_n$ Relative to Energies of Reactants $OH^- + CH_{(4-n)}Cl_n$ for $n = 1-4$

		ΔE (kJ/mol)			
n	method	aug-cc-pVDZ	aug-cc-pVTZ	aug-cc-pVQZ	CBS[a]
1	MP2	−56.1	−49.5	−47.9	−47.1
	MP3	−55.6	−50.4	−49.8	−49.5
	CCSD	−56.6	−50.2	−49.1	−48.5
	CCSD(T)	−64.0	−57.8	−56.5	−55.8
2	MP2	−61.3	−54.4	−53.1	−52.5
	MP3	−56.5	−50.5	−50.2	−50.1
	CCSD	−57.4	−50.2	−49.3	−49.0
	CCSD(T)	−68.4	−61.9	−61.0	−60.6
3	MP2	−46.5	−39.7	−38.9	−38.7
	MP3	−35.1	−28.6	−28.7	−29.0
	CCSD	−38.0	−30.3	−29.9	−29.9
	CCSD(T)	−53.5	−46.7	−46.5	−46.5
4	MP2	−4.2	−1.6	−2.0	−2.3
	MP3	9.7	12.9	12.1	11.4
	CCSD	5.9	10.2	9.9	9.6
	CCSD(T)	−10.2	−7.1	−7.9	−8.5

[a] Complete basis set limit for the relative energy is obtained by using eq 1.

TABLE 7: Barrier Heights for the Proton Transfer Reactions R2 of $OH^- + CH_{(4-n)}Cl_n$ Relative to Energies of Reactants $OH^- + CH_{(4-n)}Cl_n$ for $n = 1-2$

		ΔE (kJ/mol)			
n	method	aug-cc-pVDZ	aug-cc-pVTZ	aug-cc-pVQZ	CBS[a]
1	MP2	−45.0	−43.1	−42.7	−42.6
	MP3	−55.6	−55.1	−55.1	−55.2
	CCSD	−47.5	−45.3	−45.0	−44.8
	CCSD(T)	−51.9	−49.8	−49.4	−49.1
2	MP2	−104.2	−99.4	−99.1	−99.1
	MP3	−108.8	−105.0	−105.3	−105.6
	CCSD	−102.4	−97.1	−97.0	−97.0
	CCSD(T)	−108.0	−103.1	−102.9	−103.0

[a] Complete basis set limit for the relative energy is obtained by using eq 1.

agree to within 3.3 kJ/mol for the two smallest basis sets. The geometries of OH^- and $CH_{(4-n)}Cl_n$ in the reactant complexes are very similar to their isolated configurations, so it is no surprise that the relative energies for these systems are easy to converge. Greater differences in reaction energetics from different levels of theory are seen for the saddle points and PT product complexes, where the bonding changes from that in the isolated reactants.

The reaction energies and the relative energies of PT product complexes decrease monotonically with increasing n up to $n = 3$. The dependence upon n is surprisingly linear as shown in Figure 5. The relative energies for the reactant complexes for $n = 1$ and 2 are also shown in Figure 5. For $n = 1$ the energy of the reactant complex is slightly lower than that of the PT product complex, but for $n = 2$, the product complex is more stable by about 20 kJ/mol. Assuming that the relative energy of the reactant complex is also linear in n, the extrapolated value at $n = 3$ would be about 50 kJ/mol less stable than the product complex. The greater stability of the PT product complex for $n = 2$ and 3 and the smaller intrinsic barrier for the PT reaction for $n = 2$ are further evidence that a reactant complex does not exist for the $n = 3$ system.

For the gas-phase $OH^- + CH_3Cl$ reaction only the reaction rate for the S_N2 process has been measured, the rate constant for the PT reaction is too slow to be observed (although cross sections have been measured in studies of the translational

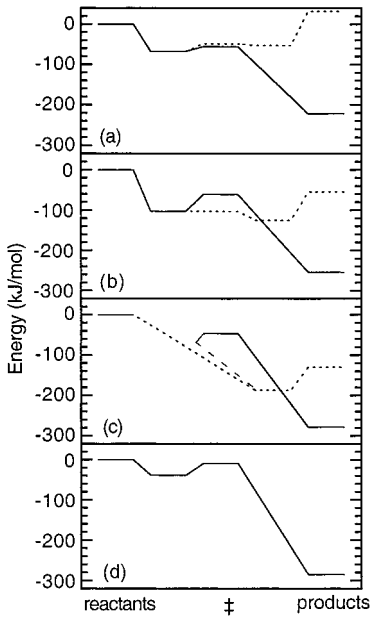

Figure 4. Relative energies (computed at the CCSD(T)/CBS level of theory) of reactant complexes, saddle points, PT product complexes, and products for the $OH^- + CH_{(4-n)}Cl_n$ reactions. Parts a−d are for $n = 1-4$, respectively. The zero of energy in each part is the reactant energy. Solid lines are for the S_N2 reactions and dashed lines are for the proton-transfer reactions. For $n = 1$ and 2, the reactant complexes are the same for the S_N2 and PT processes. Note that in part c there is no reactant complex indicated for the $CHCl_3$ reaction. As described in the text, the attack of OH^- on hydrogen in $CHCl_3$ leads to proton transfer with no barrier to the PT product complex. The S_N2 reaction does have a saddle point, but connects to the reactants through the PT product complex, which is indicated by the long-dashed line in part c.

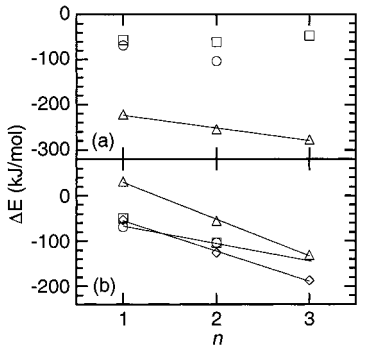

Figure 5. Energies (computed at the CCSD(T)/CBS level of theory) of critical points, relative to reactant energies, for the $OH^- + CH_{(4-n)}Cl_n$ reactions for $n = 1-3$. Part a is for the S_N2 reaction, and part b is for the PT reaction. Circles are for the reactant complexes (which are the same for the S_N2 and PT reactions), squares are for saddle points, and triangles are for the reaction energies, ΔE_{rxn}. The diamonds in part b are for the product complex for the PT reaction. Straight lines are linear fits to the data.

energy dependence of the reaction[6,7]). The energetics, as shown in Figure 4, are consistent with this finding. Note though that the threshold for the proton transfer reaction should decrease greatly with substitution of Cl for H on the methane. For $n = 2$, the S_N2 saddle point energy is −62 kJ/mol and the PT reaction energy is −56 kJ/mol, relative to reactants. For $n = 3$, the S_N2 saddle point energy increases slightly to −48 kJ/mol and the PT reaction energy decreases to −132 kJ/mol. Further studies of the threshold energies for the PT and S_N2 reactions and the branching ratios into these reaction channels for CH_2Cl_2 and $CHCl_3$ are still needed to understand the competition between these reactions.

3.3. Test of Two-Point Approximations. It is interesting that the dependence on basis set of the energies for reaction, complexes, and saddle points (shown in Tables 2−7) is similar for the different methods. Therefore, it is instructive to examine differences between these methods, since differences may converge more rapidly with respect to basis set than the individual components. That is the approach taken in eq 6 or equivalently the two-point extrapolation formula in eq 7. The factors γ^Y for each method Y and each molecule, complex, or saddle point are listed in the supplementary tables S1-S7. For each species, the value of γ^Y that is closest to the CCSD(T) value is the one for $Y =$ CCSD. Therefore, it is no surprise that the best approximation to the CBS limit for CCSD(T) absolute energies is obtained by the CCSD(T)||CCSD method. The mean unsigned differences between CCSD(T)||Y and the CCSD(T) CBS limit for the 14 molecules listed in Table 1 are 25.5, 5.3, and 1.7 kJ/mol, and the largest differences are 48.2, 10.2, and 2.8 kJ/mol, for $Y =$ MP2, MP3, and CCSD, respectively.

The performance of the two-point extrapolation formula, compared to the three-point extrapolation given by eq 1, is shown in Table 8 for the reaction energies for reactions R1 and R2. Given that the CCSD(T)||CCSD method works best for extrapolating the total energies of the molecules, it is surprising that the CCSD(T)||MP3 method gives a better approximation to the reaction energies. The average of the unsigned differences between CCSD(T)||Y and the CCSD(T) CBS results for the seven reaction energies listed in Table 8 are 0.6, 0.2, and 0.6 kJ/mol, and the largest differences are 1.4, 0.3, and 0.9 kJ/mol, for $Y =$ MP2, MP3, and CCSD, respectively. Apparently there is large cancellation of errors between the extrapolations of absolute energies for reactants and products since the mean unsigned error in the CCSD(T)||MP3 method is reduced from 5.3 kJ/mol to 0.2 kJ/mol for the reaction energies.

We also tested the CCSD(T)||Y methods for the relative energies of the reactant complex, proton-transfer complex, and S_N2 and proton-transfer saddle points. Comparison of the CCSD(T)||Y methods to the CCSD(T) CBS results are given in Table 8. For all nineteen test cases, the maximum unsigned differences of CCSD(T)||Y from the CCSD(T) CBS results are 1.4, 0.3, and 0.9 kJ/mol for $Y =$ MP2, MP3, and CCSD, respectively, and the averages of the unsigned differences are 0.4, 0.3, and 0.4 kJ/mol. The trend seen for the reaction energies is found to hold for these other energies, i.e., the CCSD(T)||MP3 method yields the best estimate of the CCSD(T) CBS results. It is very encouraging that the maximum energy difference for CCSD(T)||MP3 relative to CCSD(T) CBS is only 0.3 kJ/mol for these relative energies.

3.4. Reaction Rate Calculations. Potential energy profiles along the minimum energy path $V_{MEP}(s)$ and relative ground-state adiabatic potential curves $\Delta V_a^G(s)$ for the S_N2 reactions in the vicinity of the saddle point are shown as functions of reaction coordinate in Figure 6. All MEPs of the S_N2 reactions were followed at the MP2/aug-cc-pVDZ level of theory, using the local quadratic approximation method of Page and McIver.[33] The potential energy along the MEP, $V_{MEP}(s)$, is evaluated in the following manner. CCSD(T)/CBS energies are evaluated at the MP2/aug-cc-pVDZ critical geometries in all systems; we use the standard notation CCSD(T)/CBS//MP2/aug-cc-pVDZ to denote this level of theory. For the MEP near the S_N2 saddle point, CCSD(T)/CBS//MP2/aug-cc-pVDZ energies were calculated for a couple of geometries on either side of the saddle point for the $n = 1$ reaction. In this case the difference in the MP2 and CCSD(T) energies are nearly constant, so we apply a constant shift to the MP2/aug-cc-pVDZ energies for the MEP

TABLE 8: Comparison of Two-Point Approximations from Eq 7 Using Y = MP2, MP3, and CCSD with Complete-Basis-Set-Limit Extrapolation of CCSD(T) Using Eq 1 for Energetics of Reactions R1 and R2 of $OH^- + CH_{(4-n)}Cl_n$ for $n = 1-4$[a]

	complete basis set extrapolations of reaction energies (kJ/mol)			
	two-point			three-point
n	CCSD(T)||MP2	CCSD(T)||MP3	CCSD(T)||CCSD	CCSD(T)
S_N2 reaction energy				
1	−221.7	−221.9	−222.5	−221.8
2	−254.1	−254.6	−255.2	−254.4
3	−277.0	−277.7	−278.4	−277.5
4	−284.7	−285.3	−286.1	−285.2
PT reaction energy				
1	32.1	32.0	31.6	31.6
2	−54.2	−55.0	−55.3	−55.0
3	−128.9	−130.6	−130.9	−130.3
reactant complex				
1	−68.4	−68.2	−68.1	−67.9
2	−103.6	−103.6	−103.6	−103.2
4	−38.7	−38.7	−38.5	−38.5
PT complex				
1	−53.7	−53.3	−53.5	−53.3
2	−125.1	−125.3	−125.5	−125.1
3	−186.3	−187.3	−187.5	−186.9
S_N2 saddle point				
1	−56.1	−56.5	−56.3	−55.8
2	−60.7	−61.4	−61.1	−60.6
3	−46.3	−47.2	−47.0	−46.5
4	−8.0	−8.9	−8.6	−8.5
PT saddle point				
1	−49.6	−49.2	−49.4	−49.1
2	−103.2	−103.3	−103.3	−103.0

[a] All energies are relative to reactant energies.

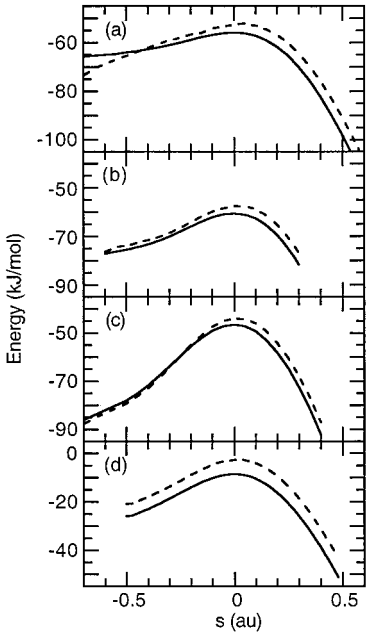

Figure 6. Potential energy profiles along the minimum energy path $V_{MEP}(s)$ (solid curves) and relative ground-state adiabatic energy curves $\Delta V_a^G(s)$ (dashed curves) as a function of reaction coordinate s for the S_N2 reactions $OH^- + CH_{(4-n)}Cl_n$ for $n = 1-4$. Parts a−d are for $n = 1-4$, respectively. Potential energy along the MEP, $V_{MEP}(s)$, is evaluated at the CCSD(T)/CBS//MP2/aug-cc-pVDZ level of theory (see text), and ground-state vibrational energy levels are approximated harmonically with frequencies evaluated at the MP2/aug-cc-pVDZ level of theory. Potential energy $V_{MEP}(s)$ is relative to the reactant energy, and $\Delta V_a^G(s)$ is given by eq 11.

around the saddle point for all the reactions. For the MEP in the asymptotic reactant region, CCSD(T)/CBS//MP2/aug-cc-pvDZ energies were calculated for several points along this portion of the MEP for the $n = 1$ reaction. $V_{MEP}(s)$ computed in this manner for the asymptotic region is not used in calculations of rate constant calculations, as described below, rather these calculations are used to validate (for $n = 1$) the electrostatic model we use for all four cases. Ground-state vibrational energy levels are approximated harmonically with frequencies evaluated at the MP2/aug-cc-pVDZ level of theory.

As seen in Figure 6, both $V_{MEP}(s)$ and $\Delta V_a^G(s)$ for $n = 1-3$ are much less than their respective values at reactants (defined to be zero for these two quantities), therefore it is unlikely that the bottleneck for these reactions will be near the saddle point. For the $n = 4$ reaction, the relative ground-state adiabatic potential is negative but much closer to zero, so the bottleneck at finite temperature for this reaction occurs near the saddle point in this case. Table 9 lists the canonical variational theory (CVT) rate constants for all S_N2 reactions, which are calculated for the dynamical bottleneck near the saddle point, and values $\Delta G^{GT}(T,s^*_{CVT})$ of the free energy of activation at variational transition states near the saddle point. The maximum in the free energy of activation curve for the CH_3Cl case is only 0.05 Å from the saddle point, and at this location $V_{MEP}(s)$ and $\Delta V_a^G(s)$ are within 0.3 kJ/mol of their saddle point values. For the other three cases the maxima in the free energy curve are less than 0.01 Å from the saddle point and $V_{MEP}(s)$ and $\Delta V_a^G(s)$ are within 0.02 kJ/mol of their saddle point values. The other columns are explained below. Note that $\Delta V_a^G(s)$ is below the asymptotic reactant energy in all cases, so we do not include any tunneling correction factors.

The proton-transfer channel for the $OH^- + CH_3Cl$ reaction is endothermic (the classical reactant energy is about 24 kJ/mol) so that the branching ratio to this channel will be negligible compared to that for the S_N2 reaction. For the reaction of OH^- with CH_2Cl_2 the reaction energy for the proton-transfer channel is comparable to the barrier for the S_N2 reaction, so the branching into the proton-transfer channel in this case may be

TABLE 9: Bimolecular Rate Constants (Units of cm^3 $molecule^{-1}$ s^{-1}) and Values of the Free Energy of Activation (Units of kJ/mol) at Variational Transition States for the Reactions of OH^- with $CH_{(4-n)}Cl_n$ ($n = 1-4$) at 300 K[a]

n	k^{CVT}	$\Delta G^{GT}(T,s^*_{CVT})$[b]	$k^{PSI-VTST}$	$\Delta G^{GT}(T,R^*_{PSI})$[c]	k^{exptl} [d]
1	7.9×10^{-4}	91	3.9×10^{-9}	122	1.5×10^{-9}
2	9.0×10^{-3}	85	3.6×10^{-9}	122	2.1×10^{-9}
3	1.8×10^{-5}	101	3.1×10^{-9}	122	2.6×10^{-9}
4	1.3×10^{-12}	142	5.5×10^{-9}	121	2.2×10^{-10}

[a] CVT rate constants for $n = 1-4$ are for the S_N2 reaction.The PSI−VTST rate constant for $n = 1$ is for the S_N2 reaction. The PSI−VTST rate constants for $n = 2-4$ are summed over all product channels. [b] Evaluated using eq 9 with $V_{MEP}(s)$ evaluated at the CCSD(T)/CBS level of theory and vibrational partition functions calculated from harmonic approximation with frequencies evaluated at the MP2/aug-cc-pVDZ level of theory. The standard state is defined as 1 cm^3 $molecule^{-1}$. [c] Evaluated using eq 9 with $V_{MEP}(s)$ evaluated from the electrostatic potential in eq 12 and partition functions for the transitional modes are obtained classically by evaluating the phase space integrals using the potential in eq 12. The standard state is defined as 1 cm^3 $molecule^{-1}$. [d] Rate constants (summed over all product channels) from the experiments of Staneke et al.[9]

appreciable. For the reaction of OH^- with $CHCl_3$ the energetics of the proton-transfer channel are favorable compared to those for the S_N2 reaction, although the relative branching ratios for the two channels will be determined by dynamics occurring after the initial dynamical bottleneck. We are mainly interested in benchmarking the electronic structure methods for the reaction energetics, which are determined by the energies at the dynamical bottlenecks so we will not pursue here dynamical calculations to determine branching ratios in the $n = 2$ and 3 cases. We report rate constants for the S_N2 reactions for $n = 1$ and 4, and total rate constants (summed over both channels) for $n = 2$ and 3.

For variational transition states with large center-of-mass separations, the potential along the MEP is dominated by electrostatic interactions (e.g., charge−dipole interactions). In these cases, we found that the potential energy surface could be adequately represented using a multipole expansion for the potential. In the electrostatic model OH^- and $CH_{(4-n)}Cl_n$ are treated as rigid molecules with charge distributions characterized by total charge, dipole moment, quadrupole moment, etc., and polarizabilities. The origin for each species is taken as its center of mass, with the molecule oriented so the *z*-axis coincides with the axis of highest symmetry (this is the required orientation in VARIFLEX). Also, we define R as the magnitude of the vector $\mathbf{R}$ from the center of mass of OH^- to the center of mass of $CH_{(4-n)}Cl_n$. Then the electrostatic potential is written through fourth order in $1/R$ as[34]

$$V_{el}(\mathbf{R},\mathbf{\Lambda}_1,\mathbf{\Lambda}_2) = -q_1\mu^2_\alpha\frac{T^1_\alpha}{R^2} + (q_1\Theta^2_{\alpha\beta} - \mu^1_\alpha\mu^2_\beta)\frac{T^2_{\alpha\beta}}{R^3} + (q_1\Omega^2_{\alpha\beta\gamma} - \mu^1_\alpha\Theta^2_{\beta\gamma} + \Theta^1_{\alpha\beta}\mu^2_\gamma)\frac{T^3_{\alpha\beta\gamma}}{R^4} + \alpha^2_{\alpha\beta}q_1\frac{T^1_\alpha T^1_\beta}{R^4} \quad (12)$$

where $\mathbf{\Lambda}_i$ is the unit vector defining the orientation of the moments of species i (with $i = 1$ and 2 for OH^- and $CH_{(4-n)}Cl_n$, respectively); q_1 is the charge on OH^- (i.e., −1); μ^i_α, $\Theta^i_{\alpha\beta}$, and $\Omega^i_{\alpha\beta\gamma}$ are the dipole, quadrupole and octapole moments for species i; $\alpha^2_{\alpha\beta}$ is the polarizability for species 2; and

$$T^1_\alpha = \frac{R_\alpha}{R} \quad (13)$$

TABLE 10: Parameters of the Electrostatic Potential of Equation 12[a]

	OH^-	CH_3Cl	CH_2Cl_2	$CHCl_3$	CCl_4
μ_x (D)	0.0	0.0	1.6649	0.0	0.0
μ_z (D)	−1.0710	1.9513	0.0	1.0811	0.0
θ_{xx} (D Å)	−5.5922	−10.0388	−14.9240	−22.2427	−27.5869
θ_{yy} (D Å)	−5.5922	−10.0388	−15.8123	−22.2427	−27.5869
θ_{zz} (D Å)	−4.1860	−8.9559	−17.0688	−21.1684	−27.5869
Ω_{xxx} (D Å^2)		−0.0048	−0.3262	0.0	0.0
Ω_{yyy} (D Å^2)		−0.1437	0.0	0.6508	0.0
Ω_{zzz} (D Å^2)		−1.2766	0.0	0.1960	0.0
Ω_{xxy} (D Å^2)		0.1437	0.0	−0.6509	0.0
Ω_{xxz} (D Å^2)		−0.1721	0.0	−0.6141	0.0
Ω_{xyy} (D Å^2)		0.0048	0.1253	0.0	0.0
Ω_{xzz} (D Å^2)		0.0	−1.0020	0.0	0.0
Ω_{yyz} (D Å^2)		−0.1721	0.0	−0.6141	0.0
Ω_{xyz} (D Å^2)		0.0	0.0	0.0	0.9717
α_{xx} (Å^3)		3.8841	5.8447	9.0003	10.0629
α_{yy} (Å^3)		3.8841	5.2148	9.0003	10.0629
α_{xx} (Å^3)		5.3939	8.1054	6.3785	10.0629

[a] $\mu_y = 0$, $\theta_{xy} = \theta_{xz} = \theta_{yz} = 0$, $\Omega_{xyz} = 0$, and $\alpha_{xy} = \alpha_{xz} = \alpha_{yz} = 0$ for all species.

$$T^2_{\alpha\beta} = \frac{3R_\alpha R_\beta}{R^2} - \delta_{\alpha\beta} \quad (14)$$

$$T^3_{\alpha\beta\gamma} = -\frac{15R_\alpha R_\beta R_\gamma}{R^3} + 3\left(\delta_{\alpha\beta}\frac{R_\gamma}{R} + \delta_{\alpha\gamma}\frac{R_\beta}{R} + \delta_{\beta\gamma}\frac{R_\alpha}{R}\right) \quad (15)$$

Dipole, quadrupole, and octapole moments were calculated at the MP2/auc-cc-pVQZ level for the OH^- molecule and MP2/aug-cc-pVTZ level for the other species. This combination of theory and basis set gave good estimates of dipole moments when compared to experimental values. The difference between calculated and experimental values for the magnitude of the dipole moment are 0.08, 0.06, and 0.07 D for CH_3Cl, CH_2Cl_2, and $CHCl_3$, respectively. Polarizabilities were calculated at the MP2/auc-cc-pVDZ level of theory for all molecules. We note that the dipole and higher moments of OH^- and the quadrupole and higher moments of the chlorinated methanes depend on the origin used in the multipole expansion. Consistent with the use of the centers of mass of OH^- and $CH_{(4-n)}Cl_n$ as the expansion points in the electrostatic potential, we use the center of mass of each species as the origin for the electronic structure calculations of the multipole moments. All calculations used the MP2 electron density.

Table 10 presents the parameters of the electrostatic potentials for OH^- interacting with $CH_{(4-n)}Cl_n$, for $n = 1-4$. Figure 7 shows the electrostatic potential as a function of center of mass separation R, in which the minimum energy is found by minimizing eq 12 with respect to orientations for each value of R. For $CH_3Cl + OH^-$, the MEP in the asymptotic reactant region was also followed starting at a C−O distance of 15 Å to map out the energy in this region of the potential energy surface. We compare the electrostatic potential along the minimum energy path with MP2/aug-cc-pVDZ and CCSD(T)/CBS//MP2/aug-cc-pVDZ energies obtained from the electronic structure calculations for the CH_3Cl reaction in Figure 7. The electrostatic potential is seen to fit the electronic structure energies extremely well over the range $R = 9-16$ Å.

The phase-space-integral-based formulation of VTST (PSI−VTST)[24] as implemented in VARIFLEX,[25] was used with the electrostatic potentials to calculate thermal rate constants at 300 K, which are reported as $k^{PSI-VTST}$ in Table 9. Values of the free energy of activation $\Delta G^{GT}(T,R^*_{PSI})$ at variational transition states in the asymptotic region of the potential are

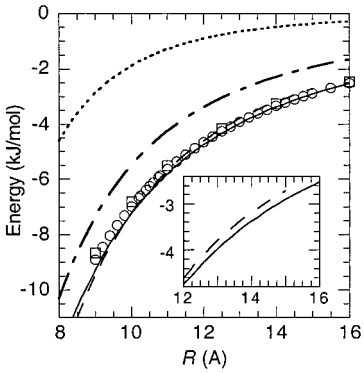

Figure 7. Electrostatic potential V_{el} from eq 12 as a function of the separation R of the centers of masses of OH^- and $CH_{(4-n)}Cl_n$, for $n = 1-4$. The solid, dashed, long−short−dashed, and dotted curves are for $n = 1$, 2, 3, and 4, respectively. The orientations of the two molecules are optimized for each R. The electrostatic potential for $OH^- + CH_3Cl$ is compared with MP2/aug-cc-pVDZ (circles) and MP2/aug-cc-pVDZ//CCSD(T)/CBS (squares) energies along the asymptotic minimum energy path. The insert repeats the $n = 1$ and 2 results for the electrostatic potential because the $n = 2$ results are obscured by the symbols in the main figure.

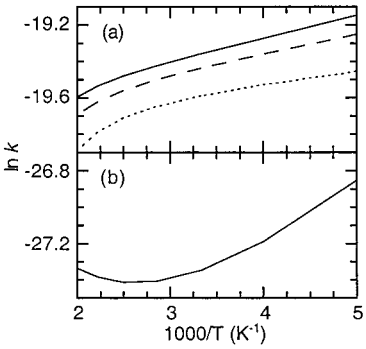

Figure 8. Temperature dependence of the rate constants for the $OH^- + CH_{(4-n)}Cl_n$ reactions with $n = 1-4$. Part a shows rate constants for the S_N2 reaction for CH_3Cl (solid curve) and total rate constants (summed over the S_N2 and PT channels) for CH_2Cl_2 (long-dashed curve) and $CHCl_3$ (short-dashed curve). Part b shows rate constants for the S_N2 reaction for CCl_4. The rate constants have units of cm^3 $molecule^{-1}$ s^{-1}.

also listed. The maxima in the free energy curves occur at $R^*_{PSI} = 12.2$, 12.4, 10.4, and 10.4 Å for the reactions with $n = 1-4$, respectively. The values of the free energy of activation in the asymptotic region are seen to be larger than those near the S_N2 saddle point for $n = 1-3$ and therefore the rate constants obtained from the PSI−VTST calculations are lower than the CVT values. Therefore, the dynamical bottlenecks for the S_N2 reactions are in the asymptotic reactant regions of the potential energy surfaces for $n = 1-3$. For the CCl_4 reaction the dynamical bottleneck is near the saddle point, even though $V_{MEP}(s)$ and $\Delta V_a^G(s)$ are below their asymptotic values. Since the values of $V_{MEP}(s)$ and $\Delta V_a^G(s)$ are close to zero, the effects of decreasing the vibrational and rotational partition functions at the generalized transition states near the saddle point (compared to transition states in the asymptotic reactant region) are more important for this reaction than for the others.

Because the dynamical bottleneck is near the saddle point for the $OH^- + CCl_4$ reaction, whereas it is in the asymptotic reactant region for the other three reactions, we expect the temperature dependence of the CCl_4 reaction to be different than for the other reactions. The temperature dependence of the four reactions is shown in Figure 8. In addition, the slopes of the curves as measured by the activation energy E_{act} in the range 250−350 K are similar: −0.8, −0.6, and −0.4 kJ/mol for the reactions with $n = 1-3$, respectively. The $OH^- + CCl_4$ reaction displays different behavior in Figure 8. First, the rate constants for this reaction are about 3 orders of magnitude lower than those for the other three reactions. Second, the slope is appreciably larger; $E_{act} = -1.6$ kJ/mol for the CCl_4 reaction in the range 250−350 K. Third, the rate constant goes through a minimum at about 400 K and has a positive activation energy for higher temperatures. The calculated PSI−VTST rate constants for the $n = 1-3$ reactions overestimate the experimental values of Staneke et al.[9] by factors of 1.2−2.6. The PSI-VIST rate constants for these three reactions are all within a factor of 1.3 of each other, while the experimental values differ by as much as a factor of 1.8. The magnitude of overestimate for the $n = 1$ reaction could be due to classical recrossing, which is known to be important for these types of S_N2 reactions,[35] and/or to inadequacies in the representation of the asymptotic potential by an electrostatic model. Note that an error of only 3 kJ/mol in the free energy of activation leads to a factor 3.3 error in the computed rate constant. The CVT rate constant for $n = 4$ underestimates the experimental rate constant by a factor of 170, which is equivalent to an error of 13 kJ/mol in the free energy of activation. Although this size of error in the barrier height cannot be totally discounted, it is larger than what we would expect from convergence of the reaction enthalpy and saddle point energy for the $n = 4$ reaction as shown in Tables 2 and 6. The differences between the CBS and aug-cc-pVQZ results for the CCSD(T) method are only 1.9 and 0.6 kJ/mol for the enthalpy and barrier height, respectively, indicating that convergence with respect to basis set is quite good. The CCSD-(T) method is expected to be quite good for these closed shell systems, and evidence for this is provided by the good agreement of reaction enthalpies for the S_N2 reactions. The difference between the computed and experimental enthalpies increases with increasing n, and this may indicate that this level of theory is becoming less accurate as more chlorine atoms are added to the system. An increase in the inaccuracy of the computed enthalpies with n may be due to insufficient tight d functions for Cl. This deficiency was pointed out in other contexts by others authors[36] and was recently addressed by Dunning, Peterson and Wilson,[37] although the new aug-cc-pV(n+d)Z sets were not used in the current work. Another source of potential error in the calculated enthalpies is the lack of scalar relativistic corrections. Higher level theoretical studies of the thermochemistry of chlorinated hydrocarbons are an interesting subject for future investigations, but are beyond the scope of the current study. We also note that the experimental error bars on the multiply chlorinated methanes are higher than those for CH_3Cl. The larger uncertainty in the experimental reaction enthalpies with increasing n is due to large error bars on the heats of formation for the chlorinated alcohols (which are obtained from calculated heats of reaction for isodesmic reactions[12]) and for the $CH_{(3-n)}Cl_n^-$ species. Nonetheless, we expect the CCSD(T)/CBS results to give reaction energetics for these systems that are accurate to within several kJ/mol. The disagreement with experiment may be partly explained by the presence of additional reaction channels, which were observed in the experiment.[9] Evidence for formation of ClO^- and CCl_3^- was seen in the low-pressure ICR experiments, although the mechanisms for production of these products are unclear.

4. Summary and Conclusions

We report accurate energetics for the reaction of OH^- with the chlorinated methanes $CH_{(4-n)}Cl_n$ for $n = 1-4$, using

Møller−Plesset perturbation theory and coupled cluster theory with augmented correlation consistent polarized valence basis sets. Using double, triple, and quadruple-ζ levels of the basis sets allow extrapolation of the computed energies to the complete basis set (CBS) limit. Experimental reaction enthalpies are accurately reproduced with three-point CCSD(T)/CBS extrapolation. In addition, we obtain excellent convergence of relative energies with respect to basis set size. For example, differences in relative energies between the triple- and quadruple-ζ results are less than 0.5 kJ/mol for reaction complexes, 1 kJ/mol for product complexes for the proton-transfer reactions, 2 kJ/mol for S_N2 saddle points, and 0.5 kJ/mol for PT saddle points. A two-point approximation to the three-point CCSD(T)/CBS extrapolations based upon MP3 calculations through quadruple-ζ level, but with CCSD(T) calculated only through triple-ζ level, give results that agree with the CBS limit to within better than 1 kJ/mol for the relative energies of all critical points on the potential energy surface.

As methane becomes more chlorinated the proton transfer reaction becomes more favorable energetically compared to the S_N2 reaction. The proton-transfer reaction is endothermic by about 24 kJ/mol for CH_3Cl, exothermic by about 62 kJ/mol for CH_2Cl_2, and exothermic by about 137 kJ/mol for $CHCl_3$. For CH_2Cl_2 the relative energy of the proton-transfer products, −56 kJ/mol, is about equal to the energy of the S_N2 saddle point, −61 kJ/mol, and for $CHCl_3$ these energies are −132 and −47 kJ/mol. Previous experiments on the CH_3Cl reactions showed that the S_N2 reaction dominated the thermal rate constants near room temperature and that the energetic threshold for the PT reaction was about 35 kJ/mol. Since the PT reactions of CH_2Cl_2 and $CHCl_3$ are exothermic, these systems offer an opportunity to study the competition between the S_N2 and PT reactions under thermal conditions, which was not afforded by the CH_3Cl system.

Calculations of rate constants for the overall reactions show that the rates are determined by dynamical bottlenecks in the asymptotic reactant region for $n = 1-3$. For the CH_2Cl_2 and $CHCl_3$ systems the PT reactions are also limited by the dynamical bottleneck in the reactant region, and the branching between the S_N2 and PT channels is determined by dynamical effects in the interaction region of the potential energy surfaces. The TST methods we use do not allow distinction of the product channels, so we have calculated total rate constants, summed over both channels, for $OH^- + CH_2Cl_2$ and $CHCl_3$. The dynamical bottleneck for the proton-transfer reaction of CH_3Cl is in the asymptotic product region and this reaction channel was not studied in detail. The computed rate constants for the reaction of OH^- with CH_3Cl, CH_2Cl_2, and $CHCl_3$ agree well with the reported experimental values. For $n = 4$ the reaction rate is controlled by a variational transition state that lies near the saddle point and larger errors are seen for the computed rate constant in this case.

Because the dynamical bottlenecks for the reactions of CH_3Cl, CH_2Cl_2, and $CHCl_3$ occur in asymptotic regions of the potential energy surface, these gas-phase reactions are not good probes of the parts of the potential energy surface near the saddle points, which control the rate constants of the solvated reactions. In subsequent work we will study the microsolvated reactions with the goal of understanding the number of solvent molecules needed to shift the dynamical bottlenecks into the saddle point regions.

Acknowledgment. The authors wish to thank Kirk Peterson for helpful discussions about the benchmark calculations, David Dixon for help with the experimental thermochemistry, and Gregory Schenter for assistance with the electrostatic model. This work was supported by the Division of Chemical Sciences, Office of Basic Energy Sciences, of the U.S. Department of Energy. This research was performed in part using the Molecular Science Computing Facility (MSCF) in the William R. Wiley Environmental Molecular Sciences Laboratory at the Pacific Northwest National Laboratory and the National Energy Research Supercomputer Center at Lawrence Berkeley National Laboratory. The MSCF is funded by the Office of Biological and Environmental Research in the U.S. Department of Energy. Pacific Northwest National Laboratory is operated for the U.S. Department of Energy by Battelle.

Supporting Information Available: Tables of all calculated total energies (at the Hartree−Fock, MP2, MP3, MP4, CCSD, and CCSD(T) levels of theory with aug-cc-pVDZ through aug-cc-pVQZ basis sets) and Cartesian geometries at the MP2/aug-cc-pVDZ level of theory are available in supplementary data. Total energies are provided for the reactants, products, reactant complexes, product complexes, and saddle points of the $OH^- + CH_{(4-n)}Cl_n$ S_N2 and PT reactions for $n = 1-4$. In addition, total energies are provided for the addition products of the nucleophilic substitution reactions $CH_{(4-n)}Cl_n + OH^- \rightarrow CH_{(3-n)}Cl_nOH + H^-$ and for the $OH^- + CH_4$ reaction. This material is available free of charge via the Internet at http://pubs.acs.org.

References and Notes

(1) Vogel, T. M.; Criddle, C. S.; McCarty, P. L. *Environ. Sci. Technol.* **1987**, *21*, 722.

(2) Schwarzenbach, R. P.; Gschwend, P. M. In *Aquatic Chemical Kinetics*; Stumm, W., Ed.; Wiley-Interscience: New York, 1990; pp 199−233. Schwarzenbach, R. P.; Gschwend, P. M.; Imboden, D. M. *Environmental Organic Chemistry*; Wiley: New York, 1993.

(3) Chabinyc, M. L.; Craig, S. L.; Regan, C. K.; Brauman, J. I. *Science* **1998**, *279*, 1882.

(4) Tanaka, K.; Mackay, G. I.; Payzant, J. D.; Bohme, D. K. *Can. J. Chem.* **1976**, *54*, 1643. Olmstead, W. N.; Brauman, J. I. *J. Am. Chem. Soc.* **1977**, *99*, 4219.

(5) Bohme, D. K.; Raksit, A. B. *J. Am. Chem. Soc.* **1984**, *106*, 3447. Henchman, M.; Hierl, P. M.; Paulson, J. F. *J. Am. Chem. Soc.* **1985**, *107*, 2812.

(6) Hierl, P. M.; Henchman, M.; Paulson, J. F. *Int. J. Mass Spectrom. Ion Processes* **1992**, *117*, 475.

(7) Hierl, P. M.; Paulson, J. F.; Henchman, M. J. *J. Phys. Chem.* **1995**, *99*, 15655.

(8) Ohta, K.; Morokuma, K. *J. Phys. Chem.* **1985**, *89*, 5845.

(9) Staneke, P. O.; Groothuis, G.; Ingemann, S.; Nibbering, N. M. M. *J. Phys. Org. Chem.* **1996**, *9*, 471.

(10) Shaik, S. S.; Schlegel, H. B.; Wolfe, S. *Theoretical Aspects of Physical Organic Chemistry*: *The S_N2 Mechanism*; Wiley: New York, 1992.

(11) Evanseck, J. D.; Blake, J. F.; Jorgensen, W. L. *J. Am. Chem. Soc.* **1987**, *109*, 2349.

(12) Bylaska, E. J.; Dixon, D. A.; Felmy, A. R. *J. Phys. Chem. A* **2000**, *104*, 610.

(13) Møller, C.; Plesset, M. S. *Phys. Rev.* **1934**, *46*, 618.

(14) Cizek, J. *Adv. Chem. Phys.* **1969**, *14*, 35. Purvis, G. D.; Bartlett, R. J. *J. Chem. Phys.* **1982**, *76*, 1910. Scuseria, G. E.; Janssen, C. L.; Schaefer, H. F. *J. Chem. Phys.* **1988**, *89*, 7382. Scuseria, G. E.; Schaefer, H. F. *J. Chem. Phys.* **1989**, *90*, 3700.

(15) Dunning, T. H., Jr. *J. Chem. Phys.* **1989**, *90*, 1007. Kendall, R. A.; Dunning, T. H., Jr.; Harrison, R. J. *J. Chem. Phys.* **1992**, *96*, 6796. Woon, D. E.; Dunning, T. H., Jr. *J. Chem. Phys.* **1993**, *98*, 1358.

(16) Peterson, K. A.; Woon, D. E.; Dunning, T. H., Jr. *J. Chem. Phys.* **1994**, *100*, 7410.

(17) Dunning, T. H., Jr.; Peterson, K. A. *J. Chem. Phys.* **2000**, *113*, 7799.

(18) Frisch, M. J.; Trucks, G. W.; Schlegel, H. B.; Scuseria, G. E.; Robb, M. A.; Cheeseman, J. R.; Zakrzewski, V. G.; Montgomery, J. A.; Stratmann, R. E.; Burant, J. C.; Dapprich, S.; Millam, J. M.; Daniels, A. D.; Kudin, K. N.; Strain, M. C.; Farkas, O.; Tomasi, J.; Barone, V.; Cossi, M.; Cammi, R.; Mennucci, B.; Pomelli, C.; Adamo, C.; Clifford, S.; Octerski, J.; Petersson, G. A.; Ayala, P. Y.; Cui, Q.; Morokuma, K.; Malick, D. K.; Rabuck, A. D.; Raghavachari, K.; Foresman, J. B.; Cioslowski, J.; Ortiz, J. V.; Stefanov, B. B.; Liu, G.; Liashenko, A.; Piskorz, P.; Komaromi, I.; Gomperts, R.; Martin, R. L.; Fox, D. J.; Keith, T.; Al-Laham, M. A.; Peng, C. Y.; Nanyakkara, A.; Gonzalez, C.; Challacombe, M.; Gill, P. M. W.; Johnson, B. G.; Chen, W.; Wong, M. W.; Andres, J. L.; Head-Gordon, M.; Replogle, E. S.; Pople, J. A. *Gaussian 98*; Gaussian, Inc.: Pittsburgh, PA, 1998.

(19) Werner, H.-J.; Knowles, P. J. MOLPRO is a package of ab initio programs written by H.-J. Werner and P. J. Knowles with contributions from J. Almlöf, R. D. Amos, A. Bernhardsson, A. Berning, P. Celani, D. L. Cooper, M. J. O. Deegan, A. J. Dobbyn, F. Eckert, S. T. Elbert, C. Hampel, G. Hetzer, T. Korona, R. Lindh, A. W. Lloyd, S. J. McNicholas, F. R. Manby, W. Meyer, M. E. Mura, A. Nicklass, P. Palmieri, K. A. Peterson, R. M. Pitzer, P. Pulay, G. Rauhut, M. Schütz, H. Stoll, A. J. Stone, R. Tarroni, P. R. Taylor, T. Thorsteinsson.

(20) Guest, M. F.; Apra, E.; Bernholdt, D. E.; Fruechtl, H. A.; Harrison, R. J.; Kendall, R. A.; Kutteh, R. A.; Long, X.; Nicholas, J. B.; Nichols, J. A.; Taylor, H. L.; Wong, A. T.; Fann, G. I.; Littlefield, R. J.; Nieplocha, J. In *High Performance Computing*: *Issues, Methods and Applications*; Dongarra, L. G. J., Joubert, G., Kowalik, J., Eds.; Elsevier Science: Amsterdam, 1995.

(21) Wigner, E. *J. Chem. Phys.* **1937**, *5*, 720. Horiuti, J. *Bull. Chem. Soc. Jpn.* **1938**, *13*, 210. Keck, J. C. *J. Chem. Phys.* **1960**, *32*, 1035. Keck, J. C. *Adv. Chem. Phys.* **1967**, *13*, 85. Garrett, B. C.; Truhlar, D. G. *J. Phys. Chem.* **1979**, *83*, 1052. Truhlar, D. G.; Garrett, B. C. *Acc. Chem. Res.* **1980**, *13*, 440. Truhlar, D. G.; Isaacson, A. D.; Garrett, B. C. In *Theory of Chemical Reaction Dynamics*; Baer, M., Ed.; CRC Press: Boca Raton, FL, 1985; Vol. IV; p 65.

(22) Garrett, B. C.; Truhlar, D. G. *J. Phys. Chem.* **1979**, *83*, 1079.

(23) Chuang, Y.-Y.; Corchado, J. C.; Fast, P. L.; Villà, J.; Hu, W.-P.; Liu, Y.-P.; Lynch, G. C.; Jackels, C. F.; Nguyen, K. A.; Gu, M. Z.; Rossi, I.; Coitiño, E. L.; Clayton, C.; Melissas, V. S.; Lynch, B. J.; Steckler, R.; Garrett, B. C.; Isaacson, A. D.; Truhlar, D. G. *POLYRATE*; 8.4.1 ed.; University of Minnesota: Minneapolis, MN, 1999.

(24) Klippenstein, S. J. *Chem. Phys. Lett.* **1990**, *170*, 71. Klippenstein, S. J. *J. Chem. Phys.* **1991**, *94*, 6469. Klippenstein, S. J. *J. Chem. Phys.* **1992**, *96*, 367. Robertson, S. H.; Wagner, A. F.; Wardlaw, D. M. *Faraday Discuss. Chem. Soc.* **1995**, *102*, 65.

(25) Klippenstein, S. J.; Wagner, A. F.; Robertson, S. H.; Dunbar, R.; Wardlaw, D. M. Variflex Software, Version 1.0; Argonne National Laboratory: Argonne, IL, 1999; (URL: http://chemistry.anl.gov/chem-dyn/Variflex).

(26) Doubleday: C.; McIver, J. W., Jr.; Page, M. *J. Phys. Chem.* **1988**, *92*, 4367. Baldridge, K. K.; Gordon, M. S.; Steckler, R.; Truhlar, D. G. *J. Phys. Chem.* **1989**, *93*, 5107. Garrett, B. C.; Koszykowski, M. L.; Melius, C. F.; Page, M. *J. Phys. Chem.* **1990**, *94*, 7096. Truhlar, D. G. In *The Reaction Path in Chemistry: Current Approaches and Perspectives*; Heidrich, D., Ed.; Kluwer: Dordrecht, 1995; pp 229−255.

(27) Langevin, P. *Ann. Chim. Phys.* **1905**, *5*, 245.

(28) Chesnavich, W. J.; Bowers, M. T. *J. Am. Chem. Soc.* **1977**, *99*, 1705. Chesnavich, W. J.; Bowers, M. T. *J. Chem. Phys.* **1977**, *66*, 2306. Su, T.; Bowers, M. T. In *Gas-Phase Ion Chemistry*; Bowers, M. T., Ed.; Academic Press: New York, 1979; Vol. 1; pp 84−117. Chesnavich, W. J.; Bowers, M. T. *Prog. React. Kinet.* **1982**, *11*, 137.

(29) Chase, M. W., Jr.; Davies, C. A.; Downey, J. R., Jr.; Frurip, D. J.; McDonald, R. A.; Syverud, A. N. *J. Phys. Chem. Ref. Data* **1985**, *14*.

(30) Pedley, J. B. *Thermochemical Data and Structures of Organic Compounds*; Thermodynamics Research Center: College Station, TX, 1994.

(31) Frenkel, M.; March, K. N.; Wilhoit, R. C.; Kabo, G. J.; Roganov, G. N. *Thermodynamics of Organic Compounds in the Gas State*; Thermodynamics Research Center: College Station, TX, 1994.

(32) Lias, S. G.; Bartmess, J. E.; Liebman, J. F.; Holmes, J. L.; Levin, R. D.; Mallard, W. G. *J. Phys. Chem. Ref. Data* **1988**, *17*.

(33) Page, M.; McIver, J. *J. Chem. Phys.* **1988**, *88*, 922.

(34) Stone, A. J. *The Theory of Intermolecular Forces*; Clarendon Press: Oxford, 1996.

(35) Hase, W. H. *Science* **1994**, *266*, 998.

(36) Bauschlicher, C. W., Jr.; Partridge, H. *Chem. Phys. Lett.* **1995**, *240*, 533. Bauschlicher, C. W., Jr.; Ricca, A. *J. Phys. Chem. A* **1998**, *102*, 8044. Martin, J. M. L. *J. Chem. Phys.* **1998**, *108*, 2791. Martin, J. M. L.; Uzan, O. *Chem. Phys. Lett.* **1998**, *282*, 16. Fast, P. L.; Truhlar, D. G. *J. Phys. Chem. A* **2000**, *104*, 6111.

(37) Dunning, T. H., Jr.; Peterson, K. A.; Wilson, A. K. *J. Chem. Phys.* **2001**, *114*, 9244.